Itinerant magnetism, electronic properties and half-metallicity of Co2ZrSn and Co2HfSn Heusler alloys

Itinerant magnetism, electronic properties and half-metallicity of Co_2ZrSn and Co_2HfSn Heusler alloys

Alessandro Difalco [1], Gabriele Barrera [2], Mauro Palumbo [1], Alberto Castellero [1,*], Marcello Baricco [1], Paola Maria Tiberto [2], and Paolo Allia [2]

[1] Dipartimento di Chimica and NIS-INSTM, Università di Torino, Via P. Giuria 7, Torino, Italy;

[2] Istituto Nazionale di Ricerca Metrologica, Strada delle Cacce 91, Torino, Italy.

* Corresponding author: alberto.castellero@unito.it, +39 0116707097, Via P. Giuria 7, 10126, Torino, Italy

Half-metallic ferromagnetic alloys are attracting considerable interest for their potential applications in spintronic devices. Co-based Heusler alloys are considered to be promising half-metallic compounds as they combine suitable magnetic, electronic and transport properties with compositional versatility and high thermal stability. In this work, Co_2ZrSn and Co_2HfSn Heusler alloys were studied by combining experimental and ab-initio investigations in order to accurately estimate their electronic density of states in proximity of the Fermi level and to determine their magnetic and electronic properties. Magnetization measurements, performed between 2 K and 550 K, suggest for both alloys a gradual transition from localized ferromagnetism to weak itinerant ferromagnetism with increasing temperature, well described by a simple mean field model up to the Curie temperature (454 K in Co_2ZrSn and 432 K in Co_2HfSn) and beyond. Ab-initio calculations were performed using two exchange-correlational functionals, PBE and PBE optimized for solids (PBEsol), in order to assess the reproducibility of theoretical results. Overall, band structures and density of states (DOS) diagrams indicated, for both compounds, the presence of a half-metallic band gap in the minority spin sub-band. The dependence of magnetic moments and band gap width on cell parameters is discussed in detail. Calculated magnetic moments and cell parameters satisfactorily match the experimental results obtained in this work and previously reported in the literature.

1. Introduction

The interest for spintronics has rapidly grown in recent years [1,2], and generation and transport of spin-polarized currents has become a decisive topic for developing suitable devices [1–4], actively stimulating research on compounds which show half-metallic properties. Among several materials [5–7], Heusler alloys, defined as ternary intermetallic compounds of X_2YZ (X, Y are transition metals, Y is a p-group element) composition and $L2_1$ space group, proved to be good candidates for spintronic applications, as they show high Curie temperature (T_C) and high spin-polarization, related to a remarkable half-metallicity [8–10]. In half-metallic Heusler alloys, the magnetization (M) is predicted to follow the Slater-Pauling rule, namely the total magnetic moment per formula unit scales with the number of valence electrons (Z) as $M_{tot} = Z - 24$. Deviations from this behavior are expected for non-perfect half-metallicity [11]. Notably, Co-based Heusler alloys were found to be suitable for spin-injection processes [12] and progressively became the focus for prospective spintronic devices operating close to room temperature. Half-metallicity was indeed reported for compounds like $Co_2FeAl_{0.5}Si_{0.5}$ [13], $Co_2Cr_{0.6}Fe_{0.4}Al$ [14], Co_2MnSi [15], Co_2CrAl [16], Co_2FeSi [17], Co_2V(Al,Ga) [18,19], and Co_2(Ti,Hf)(Si,Ge,Sn) [20,21]. Since the development of spin-voltage generators is regarded as crucial in spintronics [22,23], thermoelectric properties are also of high interest for these applications, having been proved spin-Seebeck effect to be an effective way to generate and carry spin-polarized current over relatively long distances [24]. Therefore, half-metallic alloys which show a constant, relatively large Seebeck coefficient (when compared with other thermoelectric materials [25]) and a high Curie

temperature T_C (possibly above room temperature) are greatly looked after [26]. Co-based Heusler compounds like $Co_2Ti(Si,Ge,Sn)$ and $Co_2(Zr,Hf)Sn$ have been reported to satisfy these requirements quite well [20,27]. A distinctive feature of $Co_2(Zr,Hf)Sn$ alloys is the fact that both compounds crystallize directly from the melt in the $L2_1$ structure [27], whereas the formation process of many other previously mentioned Co-based Heusler alloys, such as Co_2FeAl, Co_2FeSi, Co_2FeGa, Co_2MnAl, Co_2VAl [28] and Co_2CrAl [29], is subjected to a phase transition from a partially disordered B2 structure to the fully-ordered $L2_1$ at various temperatures. Thus, the congruent melting of the $L2_1$ structure allows an easier synthesis of the $Co_2(Zr,Hf)Sn$ alloys with respect to other Heusler, representing a potential advantage in view of potential applications.

In-depth knowledge of the nature of ferromagnetism (as determined by the electronic structure) and of the robustness of the half-metallic behaviour are crucial issues for the prospective implementation of these alloys in real devices. Information on the occurrence of band gaps at 0 K in one of the two spin sub-bands can be obtained by ab-initio calculations. On the other hand, independent information about the shape of the density of states around the Fermi level can be obtained by magnetic measurements and by the analysis of the behaviour of magnetization as a function of temperature and applied field [30–33].

In a previous work [27], we investigated structural, mechanical, and electronic transport properties of Co_2ZrSn and Co_2HfSn Heusler compounds, reporting uncommon trends of Seebeck coefficient (S), electrical conductivity and power factor (P.F.). In particular, for both alloys, the profile of S and P.F. as a function of temperature (T) was reported to be peculiar, presenting a linear growth below T_C, followed by a flat plateau above T_C. The aim of this study is to investigate the half-metallic behaviour of Co_2ZrSn and Co_2HfSn alloys, by combining experimental measurements and ab-initio calculations. The magnetic properties are discussed in terms of the Edwards-Wohlfarth model [34,35] of weak itinerant ferromagnetism using Arrott-plots [36] and checking the functional dependence of the magnetization around T_C. Experimental indications of half-metallicity are found by analyzing the magnetization dependence on temperature in both alloys. A shift from a high-temperature $M \sim T^2$ regime (Stoner law) to a low-temperature $M \sim T^{3/2}$ regime (Bloch law) was observed, and it has been attributed to a variation of the spin-flip mechanism (Stoner excitations in the first case, and transverse spin waves in the second one), suggesting the potential presence of the half-metallic band gap, as found in other Heusler alloys [30–32]. Ab-initio calculations showed the presence of a half-metallic band gap in the minority spin sub-band for both alloys. The magnitude of such band gaps and the position of Fermi energies relative to the edge of conduction bands are discussed in detail, as well as the variation of magnetic moment as a function of the lattice parameter and, as a consequence, of the choice of two different exchange-correlation functionals.

2. Experimental

Samples of Co_2ZrSn and Co_2HfSn alloys, obtained by arc-melting followed by annealing at 1073 K for 6 days, are the same used and reported in Ref. [27], where a detailed analysis of their structure and composition has already been provided. $L2_1$ Heusler was found as main phase. Small quantities of Co_2Zr and Co_2Hf C15-Laves phase were also found in Co_2ZrSn and Co_2HfSn samples, in which Sn partially substitutes Zr and Hf atoms, respectively.

Static magnetic properties were measured by means of a SQUID magnetometer (QD MPMS3) in the field interval 0 ±70 kOe, between 2 K and 400 K, and by a furnace-equipped VSM magnetometer (Lakeshore) in the field interval 0 ±17 kOe, between 300 K and 550 K, under constant Ar gas flux. Low and high temperature measurements were observed to match on the temperature interval 300-400 K, common to the two magnetometers. Small regular prism-shaped samples were used for magnetic measurements.

Ab-initio calculations were performed using Vienna Ab-initio Simulation Package (VASP) [37] with projector augmented plane (PAW) method [38]. In particular, Co, Hf_pv, Sn_d, Zr_sv potentials were adopted [39]. Perdew-Burke-Ernzerhof (PBE) [40] and Perdew-Burke-Ernzerhof optimized for solids (PBEsol) [41] functionals were selected in order to investigate the effect of computational parameters change on results. A Monkhorst-pack [42] 15x15x15 k-points mesh and Gaussian-type smearing were used for ionic relaxation

cycles, while a 24x24x24 mesh and tetrahedron-type smearing were used for single-point energy calculations. Energy cutoff of 500 eV was used in all calculations.

3. Results and Discussion

3.1) Magnetic Properties

Figure 1 shows the hysteresis loops, *M(H)*, obtained by SQUID measurements at selected temperatures between 2 K and 400 K for Co_2HfSn (panel a) and Co_2ZrSn (panel b) alloys. Both samples clearly show a non-saturating high-field behaviour, which becomes increasingly apparent at high temperatures.

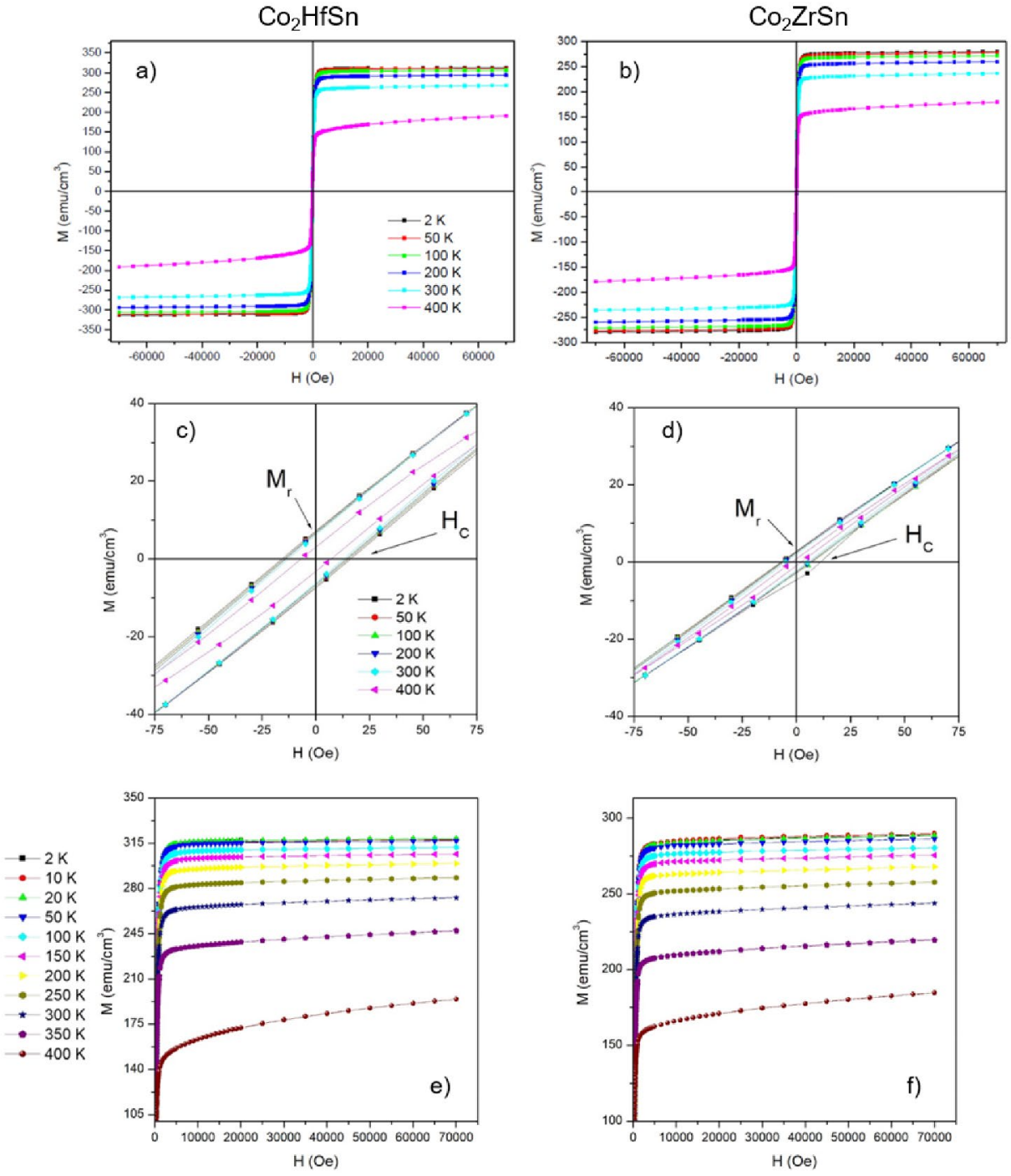

Figure 1: SQUID magnetization results. a-b) Hysteresis loops of Co_2HfSn and Co_2ZrSn, c-d) Low-field details Co_2HfSn and Co_2ZrSn, e-f) High-field details Co_2HfSn and Co_2ZrSn at different temperatures.

The low-field region of the hysteresis loops for Co_2HfSn and Co_2ZrSn alloys is highlighted in more detail in Figure 1c and 1d, respectively. A symmetric hysteresis loop is observed in both samples, with coercive field values at T = 2 K of 16 Oe for Co_2HfSn and 7 Oe for Co_2ZrSn, which gradually decreases with increasing temperature down to about 7 Oe and 2 Oe, respectively, at T = 400 K. The non-saturating high-field trend of the *M(H)* curves is highlighted in Figure 1e and Figure 1f for Co_2HfSn and Co_2ZrSn alloys, respectively.

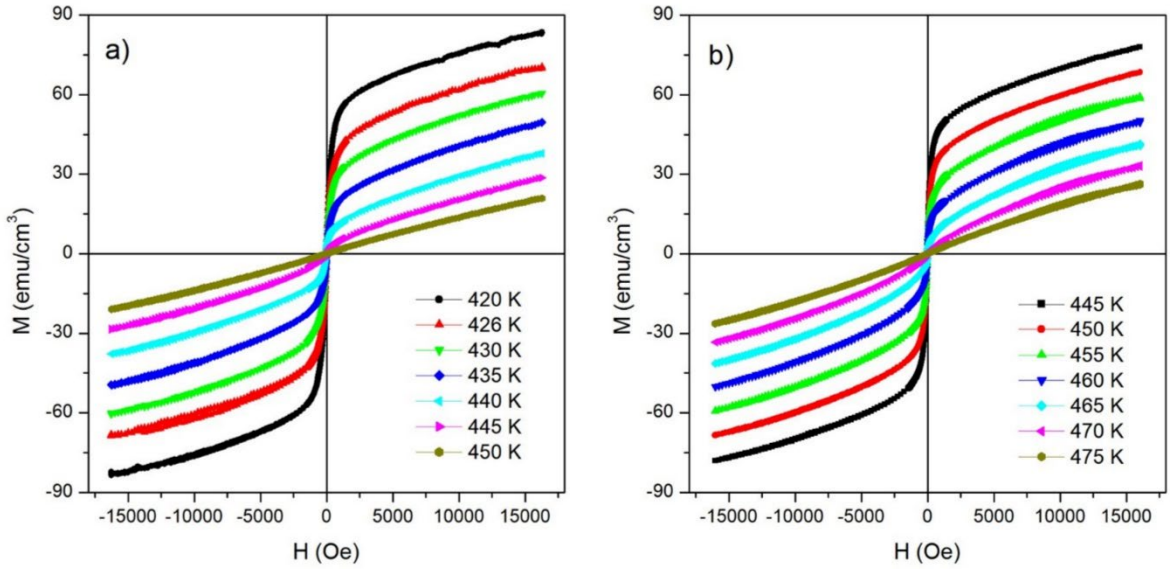

Figure 2: VSM measurements of magnetization in proximity of the Curie temperature in Co_2Hfsn (a) and Co_2ZrSn (b).

High temperature magnetic properties obtained by the VSM are shown in Figure 2 in the range around T_C. Combining SQUID and VSM measurements, it was possible to obtain the complete magnetization curve as a function of temperature under constant field (H = 5 kOe), as shown in Figure 3 for both alloys. The magnetization curves obtained by SQUID and VSM measurements match satisfactorily.

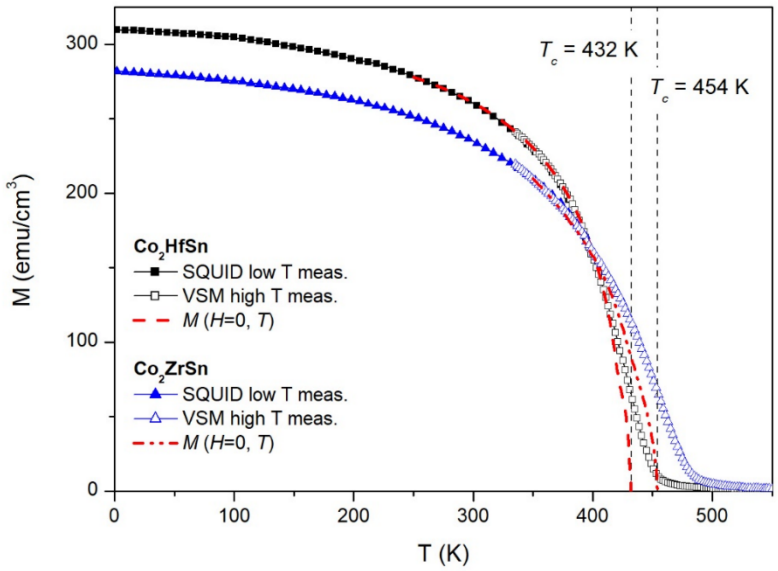

Figure 3: Temperature dependence of magnetization of Co_2HfSn and Co_2ZrSn samples under a constant field of 5 kOe. Full and open symbols refer to SQUID and VSM measurements, respectively. Red dashed lines are the corresponding *M(H=0, T)* curves derived from theory (see Section 3.2). The Curie Temperatures (T_C) are highlighted by the vertical grey dashed lines.

3.2) Weak itinerant ferromagnetism

In weak itinerant ferromagnets, the electrons responsible for ferromagnetism participate in the electrical conduction and the unbalance between spin-up and spin-down carriers is small. In Wohlfarth's simple model of weak itinerant ferromagnetism, the following relationship is obtained under equilibrium conditions for free magnetic energy [34,35]:

$$\frac{H}{M} = \alpha(T) + \beta(T)M^2 + O\{M^4\} \quad (1)$$

where *M(H,T)* is the magnetization, α, β are temperature dependent coefficients.

This expression is valid when the following two conditions are simultaneously satisfied: a) $M(H,T) \ll Nn\mu_B$, where, *N* is the number of atoms concurring to provide electrons to the conduction band, *n* the number of electrons per atom in the conduction band, μ_B is the Bohr magneton; b) $T \ll T_F$, where T_F is the Fermi temperature of the electron gas. In our case, the maximum magnetization is $M_{max} \cong 0.1nN\mu_B$, and *T* is always well below T_F for both alloys. In the present case, the terms in higher even powers of magnetization (M^{2j}, where j = 2,3,4, …) may be considered negligible, because the leading factor in the coefficient of these terms is of the type $\rho'^{2j}_F / \rho_F^{4j+1}$, where ρ_F and ρ'_F are, respectively, the density of states and its derivative at the Fermi energy [34]; these coefficients are estimated to be very small for $j \geq 2$, when the DOS $\rho(E)$ does not show a highly structured behaviour around the Fermi energy (as discussed in Section 3.3).

This model implies that the ferromagnetic order of Co_2HfSn and Co_2ZrSn compounds can be basically described by two temperature-dependent parameters, α and β (see Equation 1). These quantities can be derived from the Arrott plots, as shown in Figure 4. In weak itinerant ferromagnetism, Arrott plots directly derive from Equation 1, when $O\{M^4\}$ terms are neglected, so that a linear relationship between M^2 and H/M should be observed at all temperatures, both well below and above T_C (Figure 4). As usual [36,43,44], the low-field regions are excluded by the plot, because the Wohlfarth theory applies to an infinitely extended, ideal single crystal, containing no magnetic domain walls, whereas the low-field regions of the measured *M(H)* curves are dominated, in real samples, by the presence of multiple magnetic domains arising by effect of surfaces, grain boundaries, defects, magnetic anisotropies, and responsible for the observed magnetic hysteresis. Data shown in Figure 4 are taken for $H \geq 7$ kOe, i.e., well above the closure field of the hysteresis loops, where the sample can be assumed to be in a single-domain state. The observed linearity between M^2 and H/M at all temperatures (Figure 4a,b) strongly suggests that both compounds are indeed weak itinerant ferromagnets. It should be remarked that in all ferromagnetic materials the linearity between M^2 and H/M can usually be observed near to the Curie temperature, being derived from the general Landau's theory of magnetic phase transitions [34,36], but it is hardly found elsewhere.

The trend of the parameter $-\alpha(T)$ as a function of temperature is shown in Figure 4c. It should be noted that information about T_C can be obtained either from the graphs in panels a), b) of Figure 4 (the linear extrapolation of the high-field data is expected to pass through the origin at $T = T_C$) or from the change of sign of the parameter $-\alpha(T)$ observed in Figure 4c. The latter method allows a more accurate estimate of the transition temperature, resulting in T_C = 432 K and T_C = 454 K for Co_2HfSn and Co_2ZrSn, respectively. The theoretical zero-field magnetization for $T \leq T_C$ is $(H = 0, T) = \sqrt{-\alpha(T)/\beta(T)}$. This curve is shown in Figure 3 (red dashed line). The effect of applying a constant magnetic field (H = 5 kOe) during measurements is negligible at low temperatures (i.e., $(H = 5\ kOe, T) \cong M(H = 0, T)$) whereas it becomes increasingly apparent when T approaches to T_C and obviously for $T > T_C$. As a matter of fact, the magnetization curve at 5 kOe obtained using the SQUID magnetometer (i.e. up to 400 K) can be safely taken as representative of the behaviour of the ideal spontaneous magnetization.

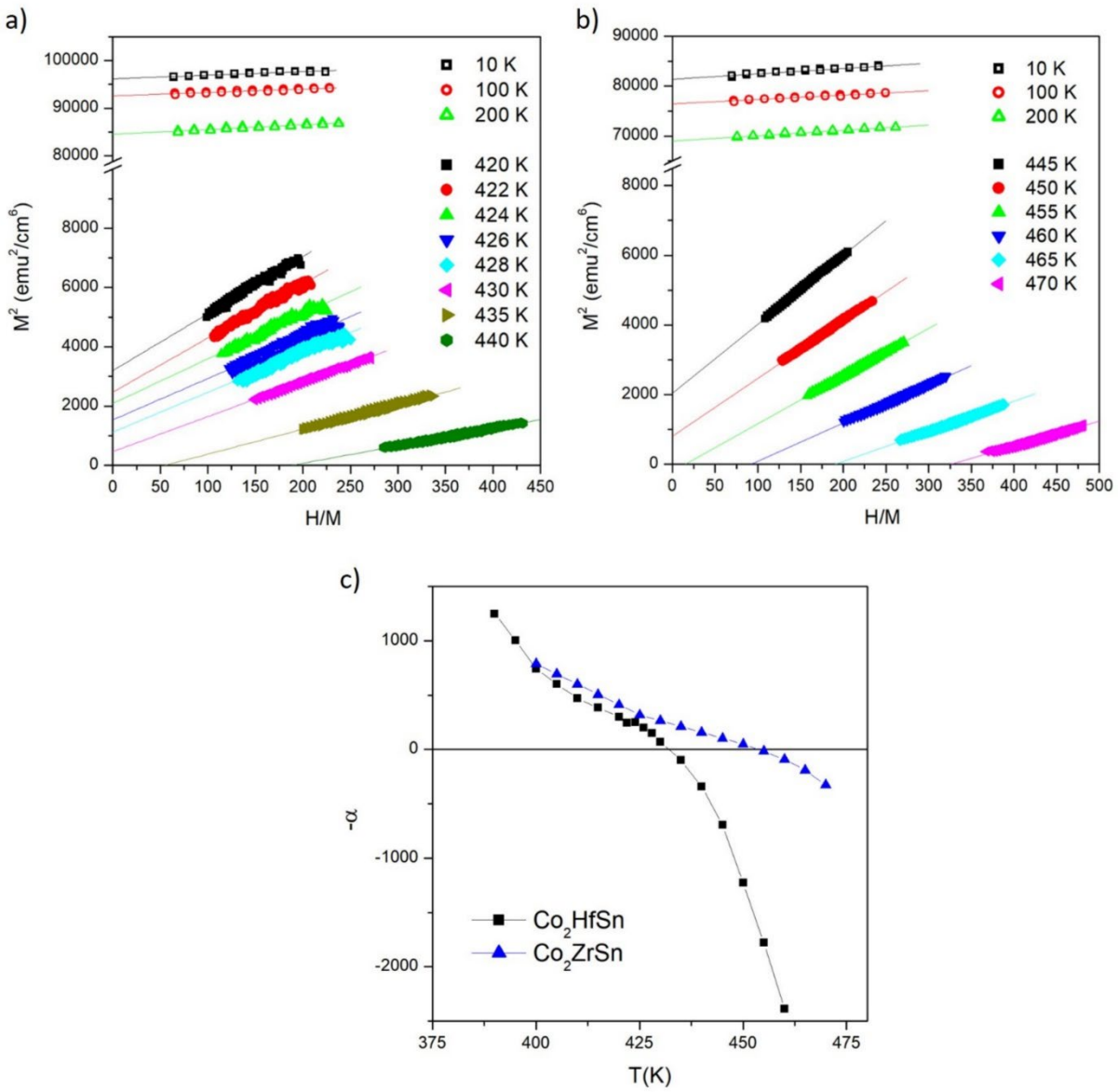

Figure 4: Arrott plot of a) Co_2HfSn, b) Co_2ZrSn alloys, and c) -α parameter as a function of temperature around T_C.

The data reported in Arrott plots are well described (even in proximity of the ferromagnetic-paramagnetic transition) by using the mean-field values for the exponents of *H/M* and *M*, as appearing in Equation 1 (i.e., 1 and 2, respectively) [21,35]. Slightly different values of the critical exponents (1.02-1.03 and 2.10-2.12, respectively) were recently found in Co_2HfSn by exploiting accurate magnetization measurements performed using a SQUID magnetometer around T_C [21].

A further method to prove that the mean field model is able to describe the magnetic properties of Co_2HfSn and Co_2ZrSn samples at high temperatures, is to verify the functional dependence of *M* on *H* near T_C. According to Equation 1, at T_C the behavior of *M* with *H* is predicted to be:

$$M(H) = \frac{1}{\beta^{1/3}(T_C)} H^{1/3} \qquad (2)$$

The $M(H^{1/3})$ curves are reported in Figure 5 for temperatures around T_C. All curves are basically linear and almost parallel to each other, as indicated by the theory, the coefficient β being almost constant there.

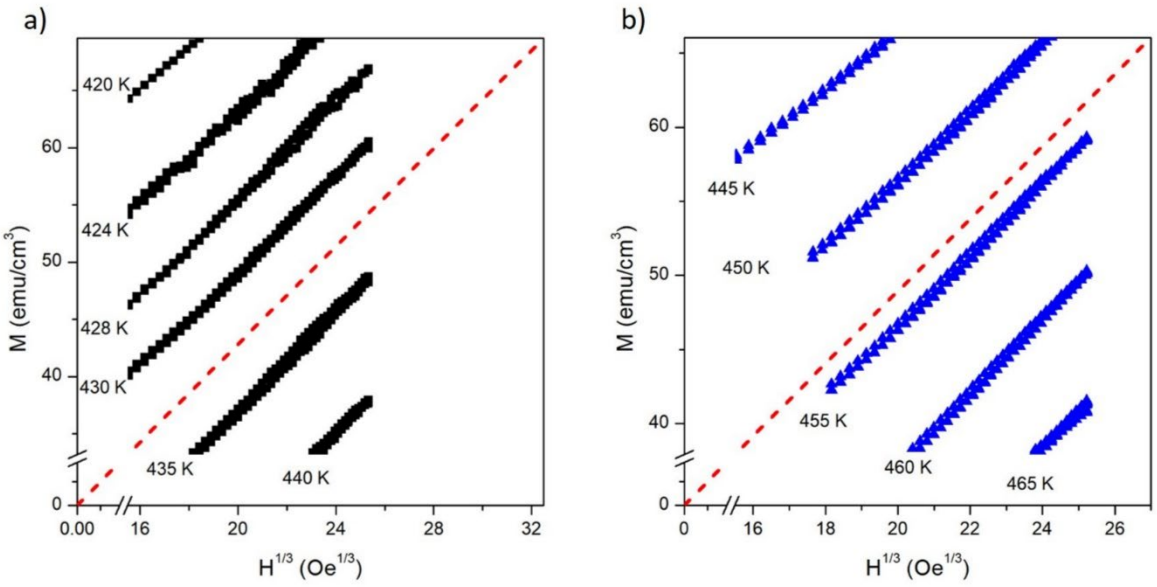

Figure 5: Symbols: experimental magnetization dependence on $H^{1/3}$ around T_C of Co_2HfSn (a) and Co_2ZrSn (b). Dashed straight lines: behavior of $M(H^{1/3})$ predicted at $T = T_C$.

The inverse initial susceptibility $\chi_0^{-1} = (\lim_{H\to 0} \frac{dM}{dH})^{-1}$ is reported as a function of $T > T_C$ in Figure 6a,b (full symbols). In the mean field model of weak itinerant ferromagnetism, $\chi_0^{-1}(T) \equiv \alpha(T)$, as directly derived from Equation 1. The quantity $\alpha(T)$ obtained from the Arrott plots is also shown in Figure 6a,b (open symbols). Experimental and predicted results are in rather good agreement well above T_C, while close to the Curie temperature the inverse magnetic susceptibility is substantially lower than the theoretical prediction, indicating that the $M(H)$ curves are steeper than predicted by the model. This can be checked by directly looking at experimental and calculated $M(H)$ isotherms (Figure 6c,d). The theoretical curves are easily obtained in analytical form by solving Equation 1, as reported in the Supplementary Material.

The curves drawn using the $\alpha(T)$ and $\beta(T)$ values derived from the Arrott plots, with no adjustable parameters, are shown in Figure 6c,d. For both compounds, all theoretical curves appear to be superimposed to the corresponding experimental results at high magnetic fields. This confirms that terms in high powers of magnetization (M^{2j}, where j = 2,3,4, …) in Equation 1 are not required in order to describe the present experimental results As it will be discussed later, this is related to the shape of the electronic density of states around the Fermi level.

Below T_C, the agreement between theory and experiment is to be expected only at high fields, when the sample is in a single-domain state (see Section 3.2). In particular, the theory predicts the existence of a finite value of the spontaneous magnetization $M(H,T)$ for $H \to 0$, whereas the presence of magnetic domains in a real sample leads to a much lower remanence value, which is very close to zero in the temperature range considered in Figure 6c,d. This explains the observed deviation between theory and experiment below about 7 kOe.

Well above T_C the agreement between theory and experiment is very good. In this case, both experimental and theoretical curves appear to be perfectly superimposed over the entire magnetic field range, including the low field region. A deviation is observed in both compounds for temperatures slightly higher than T_C; in particular, the experimental curves turn out to be steeper than predicted by the model. This behavior reflects the discrepancy of χ_0^{-1} and α values around T_C put in evidence by Figure 6a,b. One possible origin of this behavior is the presence of slight fluctuations in the composition of samples, which could entail a non-uniform transition temperature T_C in different regions of the material. In this case, the higher slope of the experimental curves for temperatures just above T_C could derive from a residual ferromagnetic contribution of regions where the magnetic transition has not yet occurred. In this regard, it should be mentioned that as far as the composition

of Heusler phases are concerned, SEM-EDS analysis of samples indicated deviations from the ideal stoichiometry, of the order of a few percent, as reported elsewhere [27].

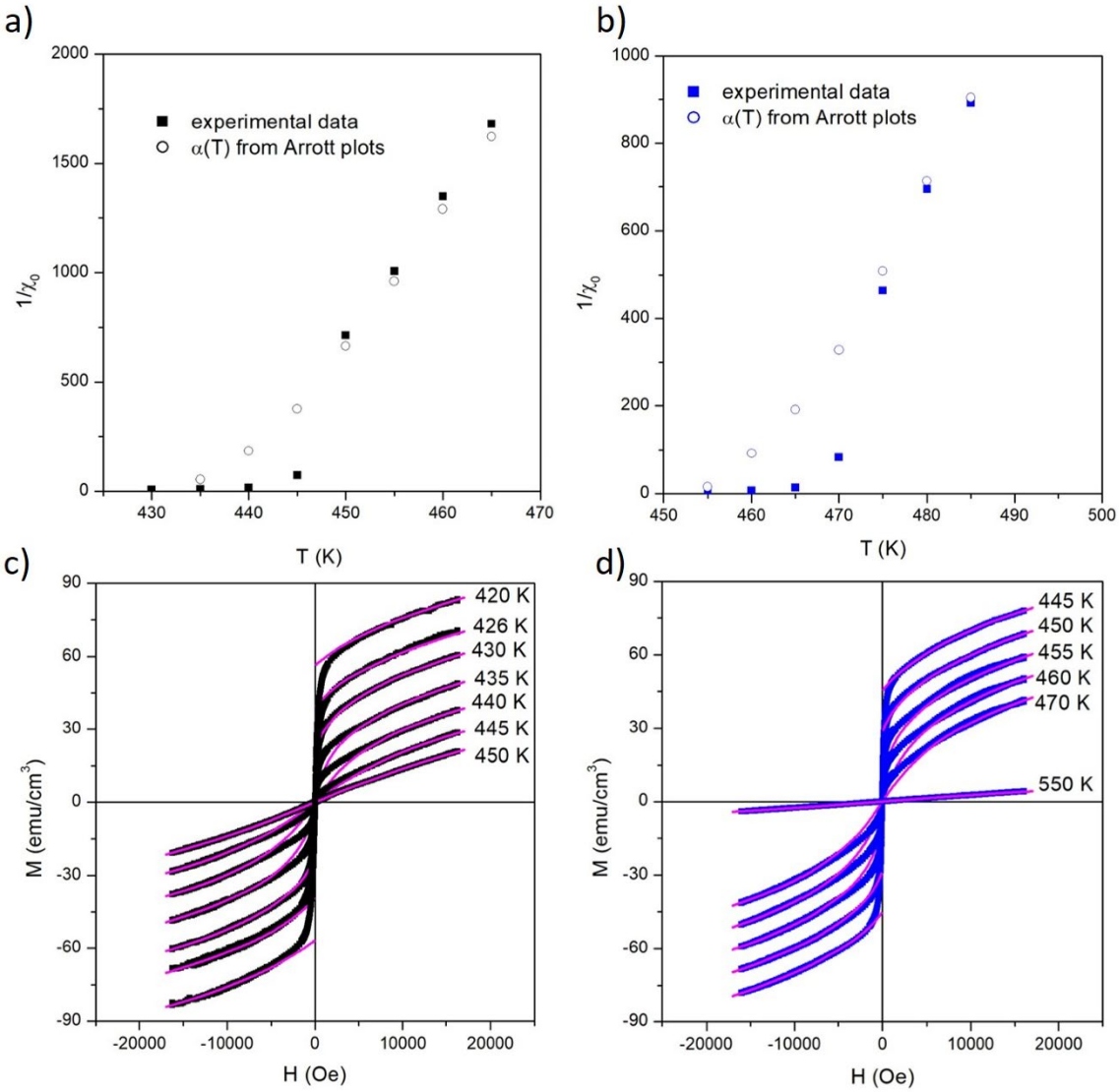

Figure 6: Upper row: inverse of the zero-field magnetic susceptibility (χ_0^{-1}) as a function of temperature in Co_2HfSn (a) and Co_2ZrSn (b). Full symbols: experiment, open symbols: theory. Lower row: comparison between experimental and calculated *M(H)* isothermal magnetization curves of Co_2HfSn (c) and Co_2ZrSn (d). Full symbols: experiment, lines: theoretical *M(H)* curves (see Section 3.2).

3.3) Ab-initio calculations

In order to better understand the nature of half-metallicity in Co_2HfSn and Co_2ZrSn, ab-initio calculations have been performed. Two exchange-correlation functionals, Perdew-Burke-Ernzerhof (PBE) and Perdew-Burke-Ernzerhof optimized for solids (PBEsol), were used with the purpose to check whether the obtained results are consistent as the simulation parameters are changed.

The total energy of the calculated cubic unit cell as a function of the lattice parameter is reported in Figure 7 for both compounds. Minimum energy values are reached for lattice parameters of 6.2498 Å and 6.1641 Å for Co_2HfSn with PBE and PBEsol, respectively, while 6.2843 Å and 6.2029 Å are obtained for Co_2ZrSn with PBE and PBEsol, respectively. Reported experimental lattice parameters [27] of 6.2157 Å for Co_2HfSn compound and 6.2458 Å for Co_2ZrSn compound, obtained at room temperature and from the same samples used in this work, are inside the calculated values. Formation energies (ΔE_{form}) per formula unit starting from the constituent elements (α-Co, α-Hf, α-Zr, β-Sn) of -1.60 eV/f.u. and -1.61 eV/f.u. were obtained using PBE

functional for Co_2HfSn and Co_2ZrSn, while, for PBEsol, ΔE_{form} values turned out equal to -1.76 eV/f.u. and -1.74 eV/f.u., respectively.

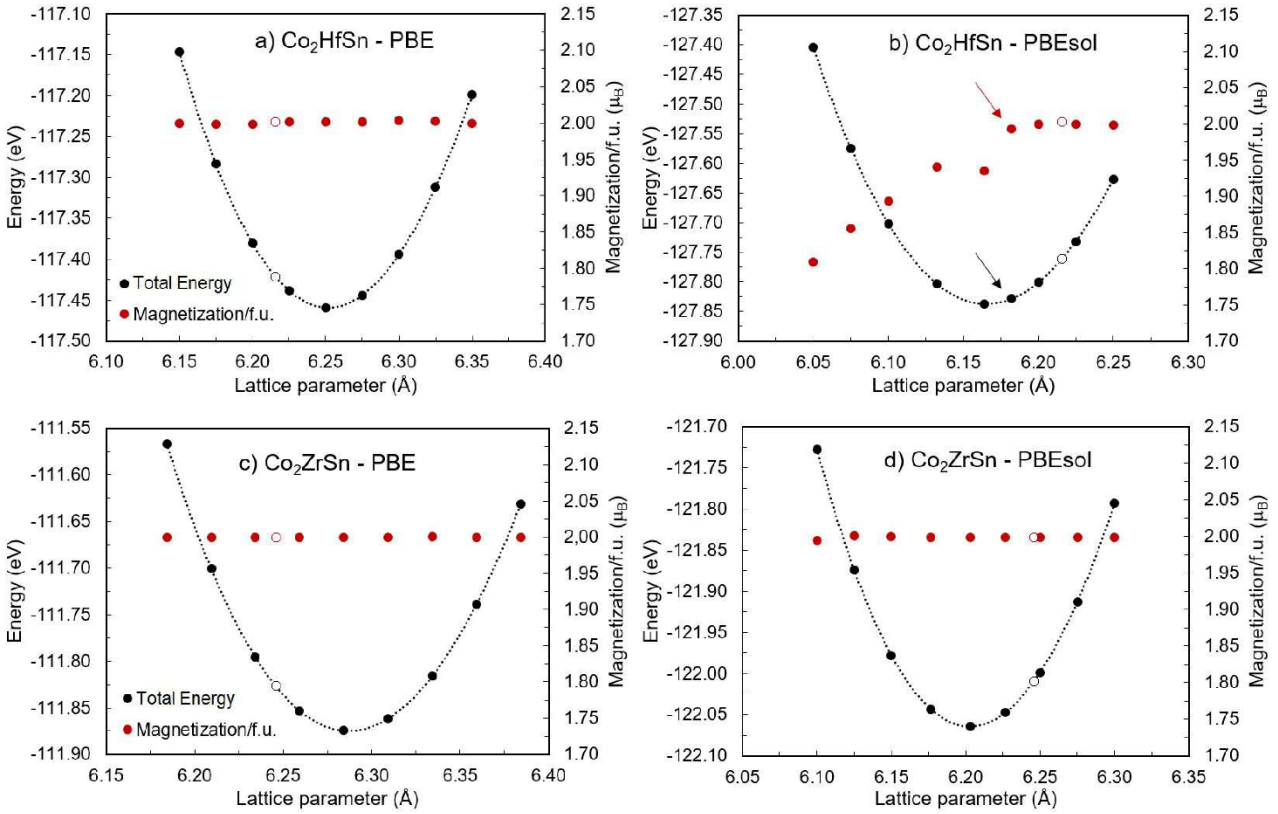

Figure 7: Total energy (black dots) and magnetization per formula unit (red dots) as a function of lattice parameter *a* (each point corresponds to results of a DFT calculation with fixed lattice parameter). a), b) Co_2HfSn computed with PBE and PBEsol, respectively. c), d) Co_2ZrSn computed with PBE and PBEsol, respectively. Empty circles are used for calculations performed imposing experimental lattice parameter values [27]. Near-equilibrium cell in Co_2HfSn-PBEsol is highlighted by arrows.

The magnetization per formula unit were also calculated as a function of the lattice parameter and results are also reported in Figure 7. For both alloys and functionals, the magnetization is generally not very sensitive to variations of *a*. An exception is Co_2HfSn when computed with PBEsol (Figure 7b) in which fluctuations up to 0.20 μ_B are observed within a range of 0.2 Å. In particular, it is notable how magnetization suddenly increases from 1.93 μ_B in the equilibrium cell (which lies at the minimum of the curve) to 2.00 μ_B in a near-equilibrium cell (highlighted by arrows), that has a lattice parameter of 6.1821 Å. Total energies and magnetic moments were also calculated imposing the above mentioned experimental lattice parameters and are indicated with empty circles in Figure 7. It can be noted that all magnetization per formula unit values are close to 2 μ_B.

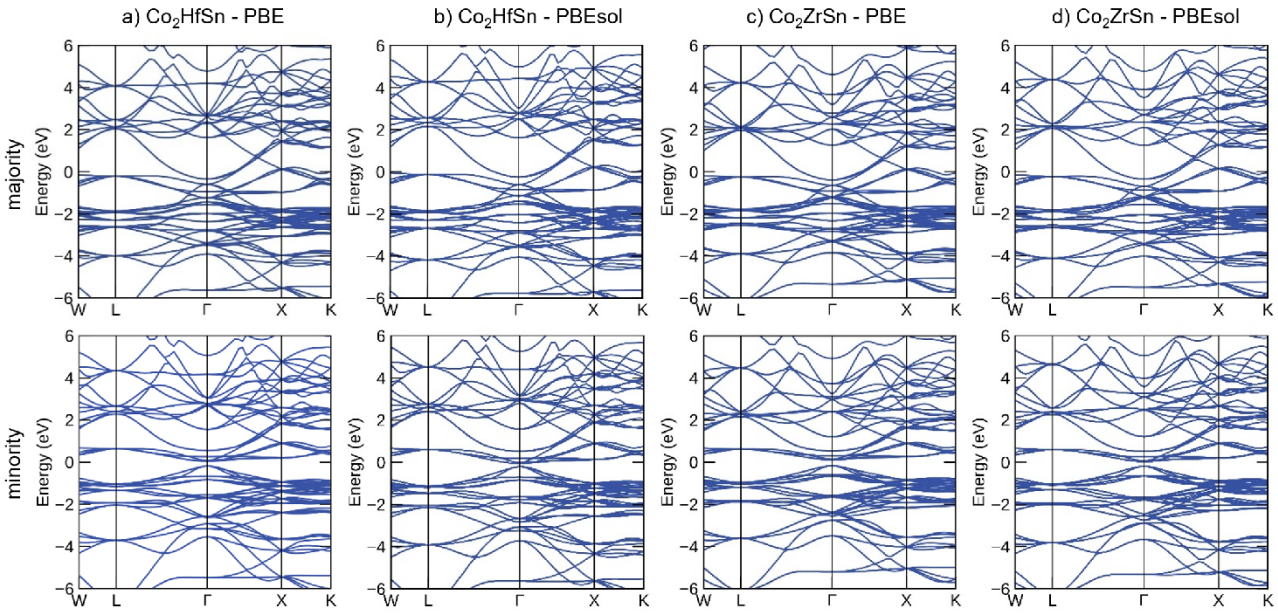

Figure 8: Band structure diagrams of Co_2HfSn alloy calculated with a) PBE, b) PBEsol functionals and Co_2ZrSn alloy with c) PBE, d) PBEsol functionals.

Calculated band structure diagrams are shown in Figure 8. It can be noted that band gaps in the minority sub-bands are direct and centred on the Γ point, while majority spin bands crossing the Fermi level are partially filled. This can be observed even more clearly from density of states diagrams, reported in Figure 9. Comparable profiles were obtained with the two functionals, both for valence and conduction levels, in majority and minority spin sub-bands. As expected for weak itinerant ferromagnets [45], majority and minority sub-bands are approximately specular and slightly shifted relative to each other.

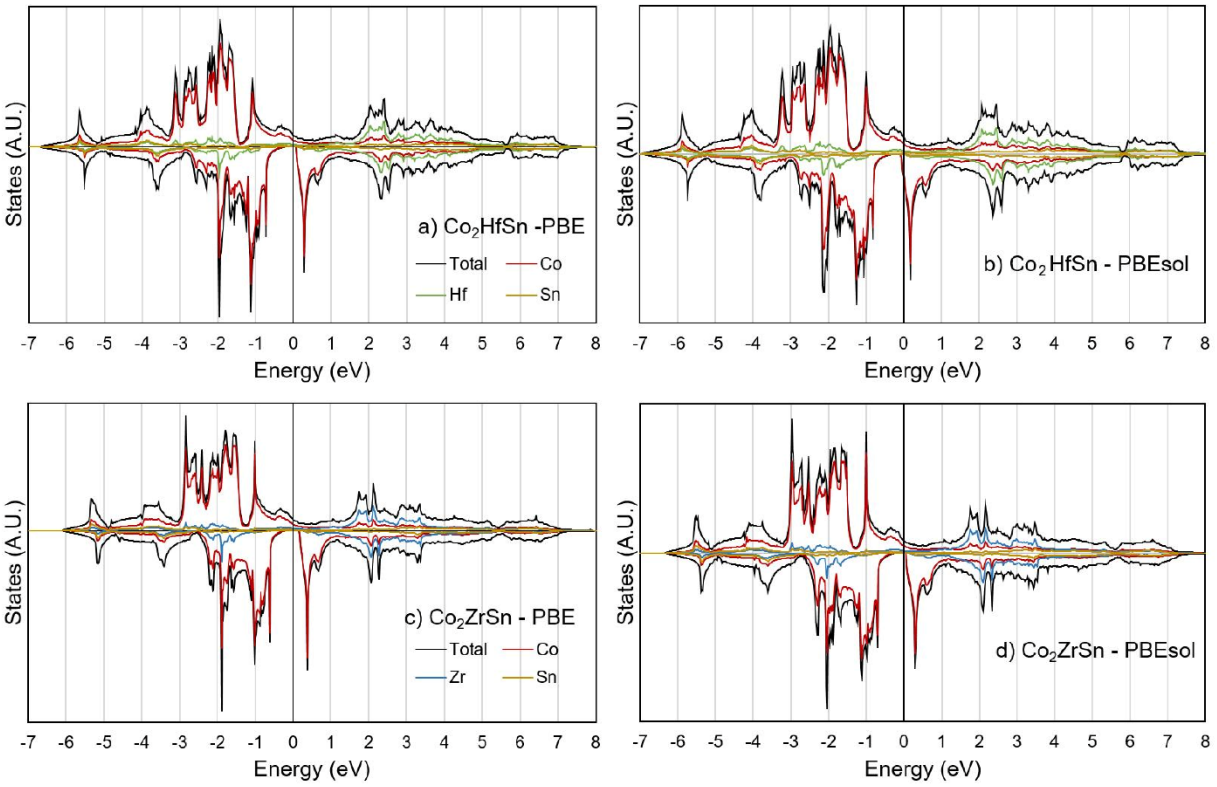

Figure 9: Total and projected density of states diagrams for the fully relaxed structures of Co_2HfSn alloy calculated with a) PBE, b) PBEsol functional and of Co_2ZrSn alloy calculated with c) PBE, d) PBEsol.

Band gaps in the minority spin sub-bands of 0.34 eV and 0.30 eV are observed for Co_2ZrSn when PBE and PBEsol are used, respectively, and the Fermi energy (E_F) is observed inside the gap. In Co_2HfSn, a band gap of 0.30 eV is obtained for PBE calculations and E_F is also observed inside the minority gap; however, when PBEsol functional is used, the Fermi energy is observed slightly outside the band gap for the minority spin sub-band. This implies that at 0 K a few electrons with minority spins have enough energy to be in the conduction band, with consequences on the calculated magnetic properties. The steep slope of the minority DOS near the Fermi energy is also particularly important as minor variations in the position of E_F can significantly change the balance between majority and minority electrons at 0 K. Values of approximately 2 μ_B (see Figure *7*) for the calculated magnetization were found in all cases, apart from Co_2HfSn computed with PBEsol, in which a 1.93 μ_B value was obtained for the fully relaxed cell. Thus, except for this latter case, the alloys are observed to follow the Slater-Pauling rule. Comparing Figure 9a with Figure 9b, and Figure 9c with Figure 9d, it can be noted that the PBEsol functional systematically locates Fermi energy of alloys closer to the conduction band. In Co_2HfSn, the position of the E_F is slightly inside the minority conduction band, causing the above-mentioned deviation from Slater-Pauling rule. The same shift of Fermi level towards the conduction band can be observed in the Co_2ZrSn DOS (Figure 9c and Figure 9d) when comparing PBE and PBEsol results; however, in this case, E_F is always inside the band gap and the resulting magnetization does not change from 2.00 μ_B.

Furthermore, as it can be noted from Figure 7b, the magnetic moment in the case of Co_2HfSn-PBEsol is also highly sensitive to small lattice parameter variations. In fact, it is noticeable how it rapidly increases up to 2.00 μ_B when increasing *a*. Increasing the fixed lattice parameter in the calculation also corresponds to a shift of the Fermi energy towards lower energies, i.e. from the conduction band to the gap in the minority sub-band. Hence, the PBEsol results for Co_2HfSn are underestimating the lattice parameter and the magnetic moment, while the position of the Fermi level is overestimated with respect to the minority band gap. This becomes evident considering the DOS diagrams shown in Figure 10 calculated using the previously mentioned experimental

lattice parameters [27] (empty circles in Figure 7). In all cases, the calculated DOS does not significantly differ from those reported in Figure 9 as well as calculated magnetic moment values, with the exception of Co_2HfSn-PBEsol (Figure 10b). In this case, Fermi energy is inside the half-metallic band gap in the minority spin sub-band and, accordingly, magnetic moment value here is 2 μ_B as in the other cases. Band-gap values for Co_2HfSn are here of 0.32 eV and 0.27 eV when calculated with PBE and PBEsol, respectively, while for Co_2ZrSn they are 0.36 eV and 0.30 eV, respectively, with PBE and PBEsol.

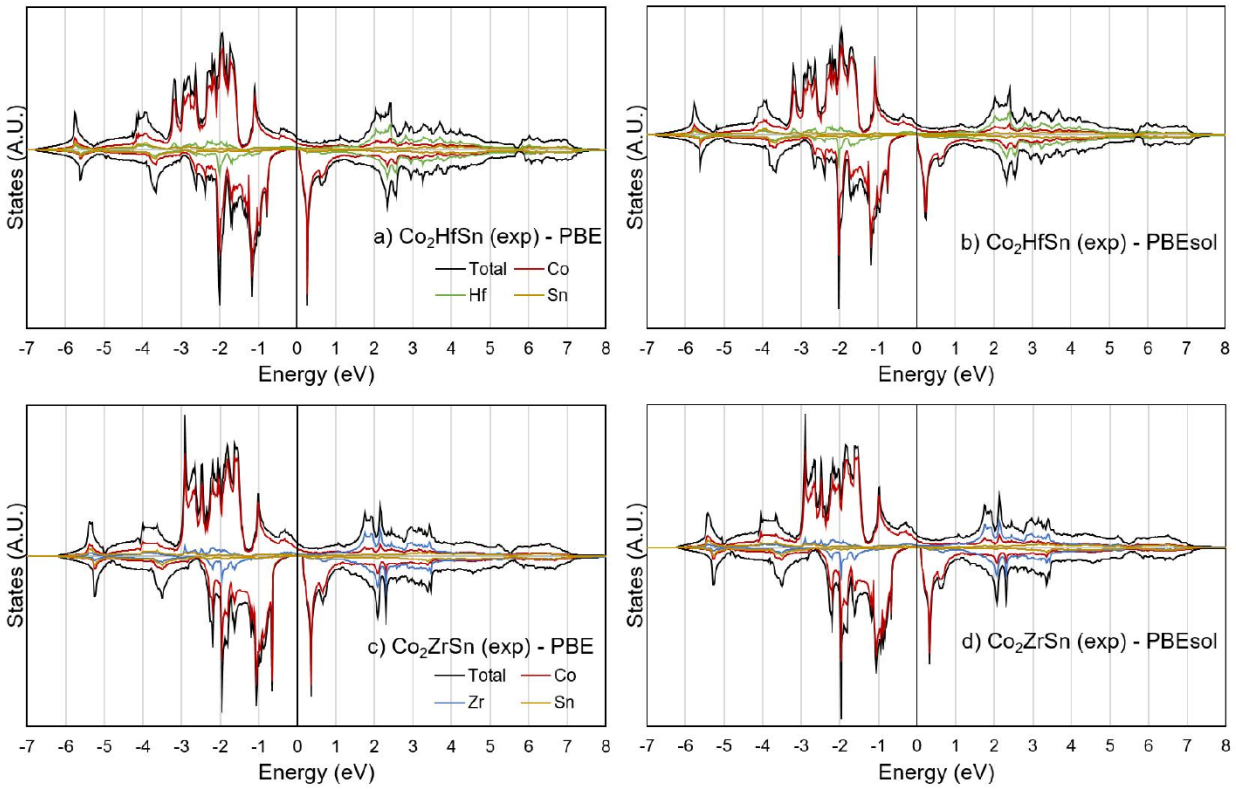

Figure 10: Total and projected density of states diagrams calculated imposing experimentally obtained lattice parameters [27] of Co_2HfSn alloy with a) PBE, b) PBEsol functional and Co_2ZrSn alloy calculated with c) PBE, d) PBEsol.

Spin-flip energy (E_{flip}), defined as the energy of the limit of minority-spin conduction band subtracted to E_F, is another important parameter that can be used in order to evaluate half-metallicity. For the equilibrium cells in Co_2ZrSn, E_{flip} are equal to 0.18 eV and 0.08 eV for calculations with PBE and PBEsol functionals, respectively. In Co_2HfSn, E_{flip} is 0.10 eV for PBE, while, for PBEsol, E_F intersects the conduction band 0.08 eV above the highest limit of the band gap. Using experimental lattice parameters, spin-flip energies are for Co_2HfSn respectively of 0.06 eV and 0.01 eV with PBE and PBEsol, while for Co_2ZrSn they are 0.16 eV and 0.12 eV with PBE and PBEsol, respectively. In all cases, Co_2ZrSn compound shows the largest E_{flip}.

As noticeable from projected DOS diagrams (Figure 9 and Figure 10), in all cases, densities of states near Fermi level are dominated by Co contribution. Also, magnetization values are due almost exclusively to Co atoms, as expected. This information suggests that tuning of half-metallic and conductive properties can be effectively achieved acting almost exclusively on Co sites.

3.4) Magnetization at low temperature

The temperature dependence of the magnetization measured under a magnetic field of 5 kOe (basically coincident with the spontaneous magnetization, as remarked before) is shown in Figure 11. In both compounds, the magnetization is accurately fitted by a law of the type $M_s = M_s(0)(1-AT^2)$ up to $T \approx 230$ K (left panels). However, at low temperatures, the $M(T^2)$ curve deviates upwards from a straight line, as shown in the two

insets of Figure 11; in Co_2ZrSn the deviation is stronger and takes place below about 70 K, whilst in Co_2HfSn it is observed below about 30 K. At low temperatures, the magnetization can be instead fitted by the Bloch law, $M_x\ (T) = M_s(0)\ (1-BT^{3/2})$, as shown in Figure 11 (right panels). These results are in good agreement with the calculated DOS (see Section 3.3) and with the possible half-metallic character of these Heusler alloys. In itinerant ferromagnets, the linear dependence of magnetization on the square of temperature arises by effect of spin flipping excitations of electrons (Stoner excitations); however, in half metals, spin-flip processes are inhibited at low temperatures by the spin-flip energy E_{flip}, so that transverse spin wave excitation, resulting in the Bloch law, becomes the dominant mechanism of magnetization reduction [30]. This effect can be pictured as the prevalence of localized (Heisenberg-type) ferromagnetism at very low temperature (as expected for half metals when spin-flip processes are inhibited) followed by a gradual transition to standard itinerant ferromagnetism, when Stoner excitations begin to play an important role.

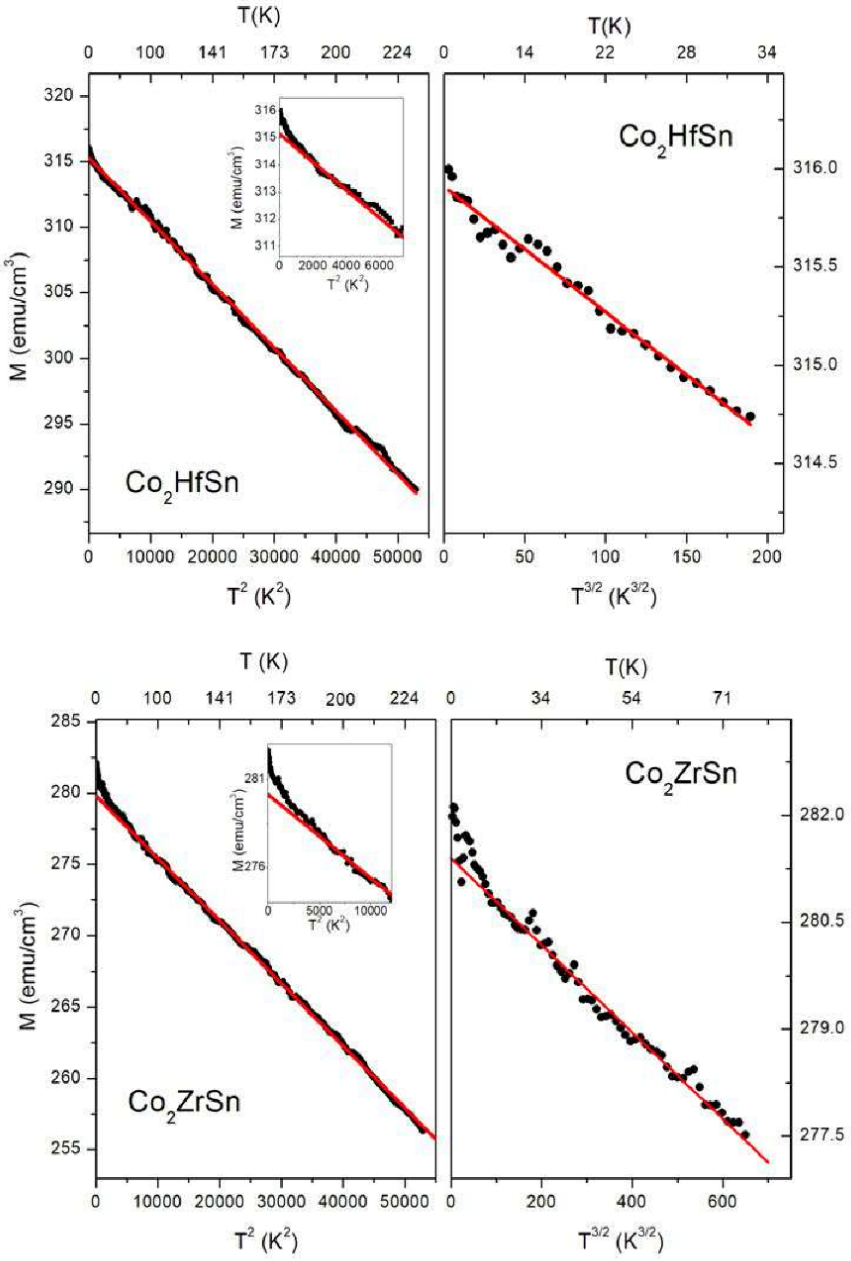

Figure 11: Left panels: Plot of spontaneous magnetization M_s as a function of T^2 in Co_2HfSn (up) and Co_2ZrSn (down). Insets show the deviation from the T^2-law. Right panels: plot of M_s as a function of $T^{3/2}$ at low temperatures in Co_2HfSn (up) and Co_2ZrSn (down).

The observed crossover between Bloch and Stoner laws for *M(T)* is in agreement with the theoretical prediction that the Fermi energy is in the gap of the minority electron sub-band. In Co_2ZrSn, the crossover temperature

is higher than in Co_2HfSn, suggesting a higher spin-flip energy, as actually predicted by calculations (Figure 9). In Co_2HfSn, the much weaker deviation of $M(T)$ away from the T^2 law is compatible with a Fermi energy still located in the minority electron gap, but very close to its upper edge, so that spin-flip processes begin to take place at very low temperatures. The picture emerging from the present analysis for Co_2HfSn agrees with the results of simulations performed using the PBE and PBEsol functionals (see Figure 9 and Figure 10) where the Fermi level was found to be remarkably close to the edge of the conduction band. It should be remarked that in the region where spin-flip effects dominate, the quantity $\Delta M/M = [M_s(0)-M_s(T^2)]/M_s(0) = A\ T^2 / M_s(0)$ turns out to have basically the same slope ($A/M_s(0) \approx 1.70 \times 10^{-6}\ K^{-2}$) in both alloys, indicating that the densities of electronic states around the Fermi level are similar in the two compounds [46], in qualitative agreement with the calculated DOS.

As far as the magnetic moments per formula unit are concerned, based on the Slater-Pauling rule for half-metallic Heusler alloys as well as ab-initio calculations (Section 3.3), values of $\mu = 2.00\ \mu_B$ are expected for these compounds. Magnetic moments of $\mu = 2.01\ \mu_B$/f.u. for Co_2HfSn and $1.80\ \mu_B$/f.u. for Co_2ZrSn result from extrapolation to $T = 0$ K of the overall experimental data. These values are in agreement with the experimental values of μ reported in different papers, ranging from 1.50 to 2.00 μ_B/f.u. in Co_2HfSn [21,47–51] and from 1.34 to 2.00 μ_B/f.u. in Co_2ZrSn [47,48,50–55]. However, the effect of the relative amount of impurities present in the samples used in this work (see Section 2) should also be taken into account. The intermetallic compounds Co_2Hf and Co_2Zr are known to be standard Pauli paramagnets, characterized by very low susceptibility values [55–57]. A calculation done using these susceptibility values shows that the contribution of the magnetic impurities is completely negligible at all temperatures, resulting in a magnetization at 70 kOe which is lower than the measured value by about three orders of magnitude. Considering the presence of the impurity phases, the values per formula unit would become: $\mu = 2.15\ \mu_B$/f.u. for Co_2HfSn and $2.05\ \mu_B$/f.u. for Co_2ZrSn. Deviations from stoichiometry and secondary phases are rarely taken into consideration in the literature on the considered alloys. However, the type and fraction of spurious non-Heusler compounds can strongly affect the experimental value of magnetic moment per unit formula, and can be deemed responsible for the very scattered experimental values of μ found in the literature as shown above. The occurrence of secondary phases in Co_2ZrSn and Co_2HfSn samples has already been reported in literature also by Yin et al., who extensively investigated formation enthalpies and other thermodynamic properties of a large number of Co-based Heusler compounds [28].

3.5) Comparison between experimental and calculated data

Combining experimental and ab-initio calculated data it is possible to obtain crucial information on half-metallicity of Co_2HfSn and Co_2ZrSn alloys. A collection of relevant data reported in this work, together with a selection of previously reported results in literature is presented in Table 1.

As it can be noticed, calculated data are generally in agreement with experimental values. In all cases, the half-metallic character of the investigated compounds has been confirmed by the present calculations, with the exception of Co_2HfSn when computed with PBEsol functional. The reason for this failure has already been discussed and is essentially related to the underestimation of the equilibrium lattice parameter of the unit cell when using this exchange-correlation functional for this system. This is also confirmed by the experimental lattice parameters in Table 1.

Although the results of present calculations are in good agreement with the experimental data, discrepancies between calculated and experimental data still occur (Table 1). The origin of these differences can be attributed to two main factors. First, computational details are known to have great influence on calculated properties [58]. The choice of the most suitable DFT exchange-correlation functional is usually regarded as the main issue in determining band gaps [59], Fermi energies [60] and magnetic moments [61]. Second, it has to be reminded that ab-initio calculations are usually performed in perfect crystals, thus the effect of intrinsic and extrinsic defects, off-stoichiometry, surfaces, secondary phases etc. is not normally taken into account. As an example, off-stoichiometric compositions and anti-site point defects were found to have great influence on the electronic properties of Co_2VAl [18] and Co_2MnSi, Co_2MnGe, Co_2CrAl half-metallic Heusler compounds [62,63]. Finally, it is also worth noting that the experimental magnetic characterizations reported in Figure 5 and Figure 6 suggest that a rather smooth profile of density of states is expected at the Fermi level for both alloys and this is confirmed by the calculated results.

Table 1: Band gap (E_g) of the relaxed structures, formation energy (ΔE_{form}) per formula unit, magnetic moment in number of Bohr magnetons per formula unit (μ), Curie temperature (T_C) and cell parameter (a) for Co_2HfSn and Co_2ZrSn alloys. Band gap of Co_2HfSn with PBEsol is indicated in brackets because the Fermi energy is not inside the minority band gap. μ values are reported both in the limit of neglected presence of secondary phases, and as they are considered Pauli paramagnets. * Ref. [21,47–51]; $ Ref. [47,48,50–55]. Values without reference are from this work.

Co_2HfSn					
	E_g (eV)	ΔE_{form}/f.u. (eV)	μ/f.u. (μ_B)	T_C (K)	a (Å)
PBE	0.30	-1.60	2.00	-	6.2498
PBEsol	(0.22)	-1.76	1.93	-	6.1641
Exp.	-	-	2.01-2.15 1.50-2.00*	432 430 [21]	6.2157 [27] 6.218 [48]
Co_2ZrSn					
	E_g (eV)	ΔE_{form}/f.u. (eV)	μ/f.u. (μ_B)	T_C (K)	a (Å)
PBE	0.34	-1.61	2.00	-	6.2843
PBEsol	0.30	-1.74	2.00	-	6.2029
Exp.	-	-	1.80-2.05 1.34-2.00$	454 448 [54]	6.2458 [27] 6.249 [48]

4. Conclusions

The magnetic and electronic properties of Co_2ZrSn and Co_2HfSn alloys were studied combining experimental investigations and ab-initio calculations. Theoretical data on the alloys were obtained by means of a plane-wave DFT approach, using two different exchange-correlation functionals (PBE and PBEsol), suitable for solid compounds. Calculated magnetic moments and densities of states suggest a half-metallic behaviour for both alloys. Overall, the calculated data were observed to be consistent when using different functionals, with the single exception of the PBEsol results for Co_2HfSn, whose Fermi level, and hence its magnetic moment, was found to be highly dependent on the variation of lattice parameter around the equilibrium value. The results of calculations were observed to be in good agreement with experimental data, both from this work and from literature. The origin of minor differences between experimental and theoretical results was analyzed and attributed to both computational and sample-dependent contributions, such as the underestimation of the calculated lattice parameter with the PBEsol functional or deviations from the ideal composition in the experimental samples. Besides, ab-initio calculations suggest that the magnetic behaviour of electrons near the Fermi level is due almost exclusively to Co atoms, suggesting that a fine tuning of the magnetic properties could be achieved by properly varying the Co content inside the alloys.

In conclusion, both alloys can be considered as weak itinerant ferromagnets over most of the investigated temperature intervals and are well described by the Edwards-Wohlfarth model, neglecting high-power terms of magnetization. This simple mean-field approach is able to explain the magnetic behaviour of both compounds over a wide range of temperatures and applied magnetic fields. The agreement between the experimental *M(H)* curves and the ones predicted by the model without making use of terms in higher powers of magnetization indicates that basically smooth profiles of the density of states are expected in proximity of the Fermi level for both compounds. The temperature dependence of spontaneous magnetization at low temperatures confirms the existence of a crossover from localized ferromagnetism to standard itinerant ferromagnetism. This can be related to a change in spin-flip mechanism possibly due to the presence of a half-metallic band gap at low temperatures as already observed for other Heusler compounds [30].

5. References

[1] A. Hirohata, K. Takanashi, Future perspectives for spintronic devices, J. Phys. D. Appl. Phys. 47 (2014) 193001.

[2] S.H. Kang, K. Lee, Emerging materials and devices in spintronic integrated circuits for energy-smart mobile computing and connectivity, Acta Mater. 61 (2013) 952–973.

[3] A. Hirohata, H. Sukegawa, H. Yanagihara, I. Žutić, T. Seki, S. Mizukami, R. Swaminathan, Roadmap for emerging materials for spintronic device applications, IEEE Trans. Magn. 51 (2015) 1–11.

[4] Y. Xu, S. Thompson, Spintronic materials and technology, CRC press, 2006.

[5] A. Zunger, S. Lany, H. Raebiger, Trend: the quest for dilute ferromagnetism in semiconductors: guides and misguides by theory, Physics (College. Park. Md). 3 (2010) 53.

[6] Q. Sun, N. Kioussis, Prediction of manganese trihalides as two-dimensional Dirac half-metals, Phys. Rev. B. 97 (2018) 94408.

[7] Q. Xu, E. Liu, W. Shi, L. Muechler, J. Gayles, C. Felser, Y. Sun, Topological surface Fermi arcs in the magnetic Weyl semimetal Co3Sn2S2, Phys. Rev. B. 97 (2018) 235416.

[8] R.A. De Groot, F.M. Mueller, P.G. Van Engen, K.H.J. Buschow, New class of materials: half-metallic ferromagnets, Phys. Rev. Lett. 50 (1983) 2024.

[9] K. Elphick, W. Frost, M. Samiepour, T. Kubota, K. Takanashi, H. Sukegawa, S. Mitani, A. Hirohata, Heusler alloys for spintronic devices: review on recent development and future perspectives, Sci. Technol. Adv. Mater. 22 (2021) 235–271.

[10] J. Chen, Y. Sakuraba, K. Yakushiji, Y. Kurashima, N. Watanabe, J. Liu, S. Li, A. Fukushima, H. Takagi, K. Kikuchi, others, Fully epitaxial giant magnetoresistive devices with half-metallic Heusler alloy fabricated on poly-crystalline electrode using three-dimensional integration technology, Acta Mater. 200 (2020) 1038–1045.

[11] I. Galanakis, P.H. Dederichs, N. Papanikolaou, Slater-Pauling behavior and origin of the half-metallicity of the full-Heusler alloys, Phys. Rev. B. 66 (2002) 174429.

[12] X.Y. Dong, C. Adelmann, J.Q. Xie, C.J. Palmstrøm, X. Lou, J. Strand, P.A. Crowell, J.-P. Barnes, A.K. Petford-Long, Spin injection from the Heusler alloy Co 2 MnGe into Al0.1Ga 0.9 As/ GaAs heterostructures, Appl. Phys. Lett. 86 (2005) 102107.

[13] R. Shan, H. Sukegawa, W.H. Wang, M. Kodzuka, T. Furubayashi, T. Ohkubo, S. Mitani, K. Inomata, K. Hono, Demonstration of half-metallicity in fermi-level-tuned Heusler alloy Co2FeAl0.5Si0.5 at room temperature, Phys. Rev. Lett. 102 (2009) 246601.

[14] K. Inomata, S. Okamura, R. Goto, N. Tezuka, Large tunneling magnetoresistance at room temperature using a Heusler alloy with the B2 structure, Jpn. J. Appl. Phys. 42 (2003) L419.

[15] L. Ritchie, G. Xiao, Y. Ji, T.Y. Chen, C.L. Chien, M. Zhang, J. Chen, Z. Liu, G. Wu, X.X. Zhang, Magnetic, structural, and transport properties of the Heusler alloys Co2MnSi and NiMnSb, Phys. Rev. B. 68 (2003) 104430.

[16] N.I. Kourov, A. V Korolev, V. V Marchenkov, A. V Lukoyanov, K.A. Belozerova, Magnetic and electrical properties of the half-metallic ferromagnets Co2CrAl, Phys. Solid State. 55 (2013) 977–985.

[17] S. Wurmehl, G.H. Fecher, H.C. Kandpal, V. Ksenofontov, C. Felser, H.-J. Lin, J. Morais, Geometric, electronic, and magnetic structure of Co2FeSi: Curie temperature and magnetic moment measurements and calculations, Phys. Rev. B. 72 (2005) 184434.

[18] T. Kanomata, Y. Chieda, K. Endo, H. Okada, M. Nagasako, K. Kobayashi, R. Kainuma, R.Y. Umetsu, H. Takahashi, Y. Furutani, others, Magnetic properties of the half-metallic Heusler alloys

Co2VAl and Co2VGa under pressure, Phys. Rev. B. 82 (2010) 144415.

[19] J. Kübler, G.H. Fecher, C. Felser, Understanding the trend in the Curie temperatures of Co2-based Heusler compounds: Ab initio calculations, Phys. Rev. B. 76 (2007) 24414.

[20] J. Barth, G.H. Fecher, B. Balke, T. Graf, A. Shkabko, A. Weidenkaff, P. Klaer, M. Kallmayer, H.-J. Elmers, H. Yoshikawa, others, Anomalous transport properties of the half-metallic ferromagnets Co2TiSi, Co2TiGe and Co2TiSn, Philos. Trans. R. Soc. A Math. Phys. Eng. Sci. 369 (2011) 3588–3601.

[21] A. Rahman, M.U. Rehman, H. Zhao, W. Liu, J. Wang, Y. Lu, K. Ruan, R. Dai, Z. Wang, X. Tao, others, Itinerant magnetism in the half-metallic Heusler compound Co 2 HfSn: Evidence from critical behavior combined with first-principles calculations, Phys. Rev. B. 103 (2021) 94425.

[22] S.A. Wolf, D.D. Awschalom, R.A. Buhrman, J.M. Daughton, von S. von Molnár, M.L. Roukes, A.Y. Chtchelkanova, D.M. Treger, Spintronics: a spin-based electronics vision for the future, Science (80-.). 294 (2001) 1488–1495.

[23] I. Žutić, J. Fabian, S. Das Sarma, Spintronics: Fundamentals and applications, Rev. Mod. Phys. 76 (2004) 323.

[24] K. Uchida, S. Takahashi, K. Harii, J. Ieda, W. Koshibae, K. Ando, S. Maekawa, E. Saitoh, Observation of the spin Seebeck effect, Nature. 455 (2008) 778–781.

[25] D. Beretta, N. Neophytou, J.M. Hodges, M.G. Kanatzidis, D. Narducci, M. Martin-Gonzalez, M. Beekman, B. Balke, G. Cerretti, W. Tremel, others, Thermoelectrics: From history, a window to the future, Mater. Sci. Eng. R Reports. 138 (2019) 100501.

[26] N.P. Ong, Recipe for spin currents, Nature. 455 (2008) 741–743.

[27] A. Difalco, F. Aversano, S. Boldrini, A. Ferrario, M. Baricco, A. Castellero, Synthesis and Characterization of Thermoelectric Co2XSn (X = Zr, Hf) Heusler Alloys, Metals (Basel). 10 (2020) 624.

[28] M. Yin, S. Chen, P. Nash, Enthalpies of formation of selected Co2YZ Heusler compounds, J. Alloys Compd. 577 (2013) 49–56.

[29] K. Hirata, X. Xu, T. Omori, R. Kainuma, Phase stability and magnetic properties in Co2Cr (Al, Si) shape memory alloys, J. Magn. Magn. Mater. 500 (2020) 166311.

[30] P. Turban, S. Andrieu, B. Kierren, E. Snoeck, C. Teodorescu, A. Traverse, Growth and characterization of single crystalline NiMnSb thin films and epitaxial NiMnSb/MgO/NiMnSb (001) trilayers, Phys. Rev. B. 65 (2002) 134417.

[31] C. Hordequin, D. Ristoiu, L. Ranno, J. Pierre, On the cross-over from half-metal to normal ferromagnet in NiMnSb, Eur. Phys. J. B-Condensed Matter Complex Syst. 16 (2000) 287–293.

[32] A. Barry, J.M.D. Coey, L. Ranno, K. Ounadjela, Evidence for a gap in the excitation spectrum of CrO2, J. Appl. Phys. 83 (1998) 7166–7168.

[33] T. Kanomata, T. Sasaki, H. Nishihara, H. Yoshida, T. Kaneko, S. Hane, T. Goto, N. Takeishi, S. Ishida, Magnetic properties of ferromagnetic Heusler alloy Co2ZrAl, J. Alloys Compd. 393 (2005) 26–33.

[34] D.M. Edwards, E.P. Wohlfarth, Magnetic isotherms in the band model of ferromagnetism, Proc. R. Soc. London. Ser. A. Math. Phys. Sci. 303 (1968) 127–137.

[35] E.P. Wohlfarth, Very weak itinerant ferromagnets; Application to ZrZn2, J. Appl. Phys. 39 (1968) 1061–1066.

[36] I. Yeung, R.M. Roshko, G. Williams, Arrott-plot criterion for ferromagnetism in disordered systems, Phys. Rev. B. 34 (1986) 3456.

[37] G. Kresse, J. Furthmüller, Efficient iterative schemes for ab initio total-energy calculations using a plane-wave basis set, Phys. Rev. B. 54 (1996) 11169.

[38] P.E. Blöchl, Projector augmented-wave method, Phys. Rev. B. 50 (1994) 17953.

[39] G. Kresse, D. Joubert, From ultrasoft pseudopotentials to the projector augmented-wave method, Phys. Rev. B. 59 (1999) 1758.

[40] J.P. Perdew, K. Burke, M. Ernzerhof, Generalized gradient approximation made simple, Phys. Rev. Lett. 77 (1996) 3865.

[41] G.I. Csonka, J.P. Perdew, A. Ruzsinszky, P.H.T. Philipsen, S. Lebègue, J. Paier, O.A. Vydrov, J.G. Ángyán, Assessing the performance of recent density functionals for bulk solids, Phys. Rev. B. 79 (2009) 155107.

[42] H.J. Monkhorst, J.D. Pack, Special points for Brillouin-zone integrations, Phys. Rev. B. 13 (1976) 5188.

[43] C.J. Schinkel, F.R. De Boer, B. De Hon, The applicability of the Stoner-Edwards-Wohlfarth model to Ni3Ga, J. Phys. F Met. Phys. 3 (1973) 1463.

[44] F.R. De Boer, C.J. Schinkel, J. Biesterbos, S. Proost, Exchange-Enhanced Paramagnetism and Weak Ferromagnetism in the Ni3Al and Ni3Ga Phases; Giant Moment Inducement in Fe-Doped Ni3Ga, J. Appl. Phys. 40 (1969) 1049–1055.

[45] J.A. Blanco, J. Pisonero, Itinerant band weak ferromagnetism from the Stoner equations, Eur. J. Phys. 20 (1999) 289.

[46] M. Shimizu, Itinerant electron magnetism, Reports Prog. Phys. 44 (1981) 329.

[47] M. Terada, Y. Fujita, K. Endo, Magnetic properties of the Heusler alloys M2XSn (M= Co or Ni, X= Zr, Nb or Hf), J. Phys. Soc. Japan. 36 (1974) 620.

[48] K.R.A. Ziebeck, P.J. Webster, A neutron diffraction and magnetization study of Heusler alloys containing Co and Zr, Hf, V or Nb, J. Phys. Chem. Solids. 35 (1974) 1–7.

[49] E. Baggio-Saitovitch, T. Butz, A. Vasquez, I. Vincze, F.E. Wagner, K. Endo, Hyperfine fields in Co-based Heusler alloys, Le J. Phys. Colloq. 37 (1976) C6--417.

[50] P.G. Van Engen, K.H.J. Buschow, M. Erman, Magnetic properties and magneto-optical spectroscopy of Heusler alloys based on transition metals and Sn, J. Magn. Magn. Mater. 30 (1983) 374–382.

[51] R. V Skolozdra, Y. V Stadnyk, Y.K. Gorelenko, E.E. Terletskaya, Influence of vacancies on the magnetic and electrical properties of Heusler phases Me'Co2-xSn (Me'= Ti, Zr, Hf), Sov. Physics. Solid State. 32 (1990) 1536–1538.

[52] A. Ślebarski, A. Jezierski, M. Neumann, S. Plogmann, Influence of vacancies on the electronic structure of CoZrSn Heusler alloys, Eur. Phys. J. B-Condensed Matter Complex Syst. 12 (1999) 519–523.

[53] A. Yamasaki, S. Imada, R. Arai, H. Utsunomiya, S. Suga, T. Muro, Y. Saitoh, T. Kanomata, S. Ishida, Orbital angular momentum and interpretation of core-absorption magnetic circular dichroism on the band picture in Co-based Heusler alloys Co2YSn (Y= Ti, Zr, and Nb), Phys. Rev. B. 65 (2002) 104410.

[54] W. Zhang, Z. Qian, Y. Sui, Y. Liu, W. Su, M. Zhang, Z. Liu, G. Liu, G. Wu, Magnetism and Hall effect of the Heusler alloy Co2ZrSn synthesized by melt-spinning process, J. Magn. Magn. Mater. 299 (2006) 255–259.

[55] T. Kanomata, Y. Amako, Y. Ida, Y. Adachi, T. Osaki, T. Eto, H. Nishihara, I. Shigeta, S. Imada, M. Doi, Magnetic properties of ferromagnetic Heusler alloy Co2ZrSn, J. Phys. Chem. Solids. (2022) 110635. https://doi.org/https://doi.org/10.1016/j.jpcs.2022.110635.

[56] K.H.J. Buschow, Differences in magnetic properties between amorphous and crystalline alloys, J. Appl. Phys. 53 (1982) 7713–7716.

[57] H. Fujii, F. Pourarian, W.E. Wallace, Appearance of spontaneous ferromagnetism in non-stoichiometric ZrCo2, J. Magn. Magn. Mater. 24 (1981) 93–96.

[58] D. Rappoport, N.R.M. Crawford, F. Furche, K. Burke, Which functional should I choose?, Comput. Inorg. Bioinorg. Chem. 594 (2008) 1–25.

[59] P. Mori-Sánchez, A.J. Cohen, W. Yang, Localization and delocalization errors in density functional theory and implications for band-gap prediction, Phys. Rev. Lett. 100 (2008) 146401.

[60] T. Hadji, H. Khalfoun, H. Rached, Y. Guermit, A. Azzouz-Rached, D. Rached, DFT study with different exchange-correlation potentials of physical properties of the new synthesized alkali-metal based Heusler alloy, Eur. Phys. J. B. 93 (2020) 1–10.

[61] D.J. Singh, J. Ashkenazi, Magnetism with generalized-gradient-approximation density functionals, Phys. Rev. B. 46 (1992) 11570.

[62] S. Picozzi, A. Continenza, A.J. Freeman, Role of structural defects on the half-metallic character of Co2MnGe and Co2MnSi Heusler alloys, Phys. Rev. B. 69 (2004) 94423.

[63] Y. Miura, K. Nagao, M. Shirai, Atomic disorder effects on half-metallicity of the full-Heusler alloys Co2(Cr1- xFex)Al: A first-principles study, Phys. Rev. B. 69 (2004) 144413.